Controlled Demolition and Reconstruction of Imidazolate and Carboxylate Metal-Organic Frameworks by Acid Gas Exposure and Linker Treatment

Arvind Ganesan,[a] Stephen Purdy,[b] Souryadeep Bhattacharyya,[a] Katharine Page,[b,c] David S. Sholl,[a] and Sankar Nair[a]

[a]School of Chemical & Biomolecular Engineering, Georgia Tech, Atlanta, GA 30332, USA.
[b]Neutron Scattering Division, Oak Ridge National Laboratory, Oak Ridge, TN 37831, USA.
[c]Tickle College of Engineering, University of Tennessee, Knoxville, TN 37996, USA.

* Corresponding author: sankar.nair@chbe.gatech.edu, david.sholl@chbe.gatech.edu

Keywords: MOFs, acid gas, recovery

Abstract

The metal-linker coordination bond in Metal-Organic Frameworks (MOFs) can be unstable in humid and acid gas environments, leading to loss of crystallinity and porosity. This degradation is not necessarily irreversible; solvent-assisted crystal redemption (SACRed) has been shown to recover physical and chemical properties of ZIF-8 exposed to humid SO_2. This approach can be useful in creating mixed linker materials that might be challenging to produce via *de novo* synthesis. In this paper we extend the concept of controlled degradation of a MOF with acid gas, followed by treatment with a fresh linker solution to several MOF templates (ZIFs, UiO-66 and UiO-67) and acid gases (SO_2 and NO_2 in dry and humid conditions). Significant loss in porosity and crystallinity along with functional changes are observed in acid gas exposed MOFs. SACRed is shown to heal acid gas-exposed MOFs with near-complete structural and functional recovery. X-ray Pair Distribution Function (PDF) analysis confirms the molecular level degradation upon exposure with acid gas and recovery while treated with native-linker solution. These findings indicate the generality of SACRed as a means for treating a variety of MOFs.

Introduction

Metal-Organic Frameworks (MOFs) are a large and well-known class of crystalline nanoporous materials composed of metal ions coordinated by organic linkers. There is a very extensive literature investigating the synthesis and properties of MOFs relevant to separations, catalysis, storage, chemical sensors, drug delivery, and many other potential applications. In this context, the interactions of MOFs with acid gases such as SO_2, NO_2, H_2S, and CO_2, have recently generated increased interest[1–10]. The metal-linker coordination bond is often unstable in humid[11] and acid gas[1] environments. Cleavage of this bond by an acid gas species (which may occur even at ppm levels of the gas) leads to loss of crystallinity, pore size and volume due to defects in the form of acid-linker complexes[2,12]. Such degradation of MOFs was widely assumed to be irreversible[13]. However, recent studies have expanded the understanding of degradation mechanisms[2], quantifying progressive degradation,[1] and developing stability prediction capabilities by techniques such as data-driven models (correlations)[5], machine learning[14], and atomistic/quantum chemistry (DFT) calculations[15,16]. Among different MOF classes, zeolitic imidazolate frameworks (ZIFs) have been extensively studied. One such effort evaluated the stability of 16 ZIFs towards SO_2 and CO_2 in both humid and dry conditions[1], as well as the remarkably different effects of NO_2 and SO_2 on ZIFs[3]. ZIFs were observed to have different stabilities towards SO_2 and NO_2 in dry environments and in the presence of humidity. ZIFs are stable in dry SO_2 and most ZIFs degrade in humid SO_2. However, degradation of ZIFs can occur in dry NO_2[3]. A detailed mechanism based

on FTIR data and DFT calculations proposed H-abstraction by free radical NO_2 followed by an acid attack of HNO_3 on metal-linker bond, whereas such a route is absent in the SO_2 case.

Recently, it was shown that acid gas damage in ZIFs can be reversed with a method named "Solvent-Assisted Crystal Redemption" (SACRed)[13] by treating the damaged ZIF with a solution of the fresh linker. In particular, ZIF-8 exposure to humid SO_2 led to significant loss of surface area, porosity and crystallinity, but post-SACRed ZIF-8 recovered structural and chemical properties nearly identical to the pristine ZIF-8. NMR and other techniques confirmed that SACRed is a true linker replacement process in which degraded linker-acid complexes were replaced by fresh linker molecules. It was also shown that SACRed could be adapted to synthesize new mixed-linker ZIFs. First, the ZIF-8 "template" MOF materials were subjected to controlled demolition by different levels of humid SO_2 exposure. Then, the partially demolished ZIF-8 materials were treated with a solution of non-native linkers to reconstruct the materials in the form of mixed-linker ZIFs that retain the same crystal topology as ZIF-8.[17] With this approach several bulky non-native linkers (benzimidazole, methylbenzimidazole, and halobenzimidazole) could be introduced into ZIF-8 while maintaining the SOD topology. Such mixed-linker ZIFs containing linkers of disparate nature are difficult to obtain by techniques such as direct (*de novo*) mixed-linker synthesis[18] or solvent-assisted linker exchange (SALE).[19] Thus, it was possible to circumvent the thermodynamic, steric, and kinetic barriers that exist for synthesis of mixed-linker MOFs using disparate types of linkers.

The above findings demonstrated ways to recover the properties of acid gas-degraded MOFs and also to synthesize new mixed linker MOFs by controlled degradation of a template MOF by an acid gas followed by insertion of non-native linkers at the degraded sites. However, almost all the early work was done with ZIF-8 as the template MOF and humid SO_2 as the demolition agent. In

this paper we focus on expanding SACRed for MOF recovery to a wider set of MOF materials and demolition agents. Specifically, we show the extension of this method to five different MOF materials (ZIF-8, ZIF-90, ZIF-71, UiO-66 and UiO-67) from the ZIF (imidazolate linkers) and UiO (dicarboxylate linkers) classes that have varied structural features and properties, using SO_2 and NO_2 in dry or humid conditions as demolition agents. SACRed recovery protocols were developed for each combination of MOF and degradation conditions. X-ray diffraction (XRD), Fourier-transform infrared spectroscopy (FTIR), and nitrogen physisorption isotherms were used to qualitatively and quantitatively study the controlled demolition and reconstruction process. We also illustrate the application of synchrotron x-ray crystallography and pair distribution function analysis to obtain molecular/unit-cell level insights on the MOF recovery process. Hence, this paper provides a proof of concept for generalizing the above-mentioned MOF recovery and new MOF synthesis approaches.

Experimental Methods

Materials

Zinc nitrate hexahydrate (Alfa Aesar), Zinc acetate (J.T. Baker Chemicals), Zirconium chloride (Sigma Aldrich), benzenedicaboxylic acid (Sigma Aldrich), 2-methylimidazole (2-MeIm) (Sigma Aldrich), imidazole-2-carboxaldehyde (OHC-Im) (Alfa Aesar), 4,5-dichloroimidazole (dClIm) (Sigma Aldrich) sodium formate (Alfa Aesar), terephthalic acid (TPA) (Acros Organics), benzoic acid (Sigma Aldrich), methanol (VWR), acetone (VWR), N, N-dimethylformamide (BDH), and Biphenyl-4,4′-dicarboxylic acid (BPDC) (TCI Co. Ltd.) were used as received. Deionized water from the EMD Millipore water purification system, 1000 ppm SO_2 balance N_2, 1000 ppm NO_2 balance N_2 and ultra-high purity air (76.5–80.5% N_2, 19.5–23.5% O_2) from Airgas were used in this work.

MOF Synthesis

ZIF-8 was synthesized with a modified procedure from Zhang et al[20]. 0.297 g $Zn(NO_3).6H_2O$ was dissolved in 20 mL methanol. Typically, 0.164 g 2-MeIm was dissolved in 20 mL methanol with 0.269 g HCOONa. The metal solution was added to the linker solution and transferred to a Teflon liner. The liner was then sealed inside a Parr Instruments stainless steel autoclave and then incubated at 363 K for 48 hours. The crystals were centrifuged at 8500 rpm for 5 mins and washed thrice with fresh methanol. The crystals were air dried at 333 K. Dried crystals were then degassed at 453 K in vacuum overnight.

Previously reported ZIF-90 synthesis protocols[21] were modified. Typically, 15.368 g of OHC-Im was added to 400 mL DMF and heated to 333 K to dissolve the linkers. 11.904 g of $Zn(NO_3).6H_2O$ was added to the solution and heated to 393 K in an oil bath for 20 min. The solution was then cooled to ambient temperature and left to crystallize for 4 days. The crystals were centrifuged at 8500 rpm for 5 mins and washed thrice with DMF. The collected crystals were washed three times with methanol and air-dried at 333 K. Dried crystals were then degassed at 453 K in vacuum overnight.

Previously reported ZIF-71 synthesis protocols[22] were modified. Typically, 0.297 g of $Zn(OAc)_2$ and 0.876 g 4,5-dichloroimidazole were dissolved in 60 mL of methanol separately. The metal solution was added to the linker solution and kept without stirring for 24 h under ambient

conditions. The collected crystals were washed three times with methanol and air-dried at 333 K. Overnight activation of crystals after air-drying was carried out by degassing in vacuum at 453 K.

UiO-66 synthesis protocol was carried out as reported earlier.[23] Typically, 0.180 g of $ZrCl_4$, 0.129 g of terephthalic acid, 14 mg deionized water were added to 30 mL of pre-treated DMF. The solution was ultrasonicated for 10 mins and heated in an oil bath at 393 K for 48 hr. The crystals were collected by centrifuge, washed thrice with DMF followed by solvent exchange with acetone to remove trapped solvent. Overnight drying at 333 K removes most acetone. The sample was activated overnight at 453 K in vacuum.

A synthesis method for UiO-67 was taken from earlier work[24]. Typically, 2.167 g of $ZrCl_4$ was added to 216 mL DMF with 503 μL of water at room temperature. The solution was heated and 0.862 g of benzoic acid was added, waited until $ZrCl_4$ completely dissolved. 2.256 g of BPDC was added. The synthesis was performed at 403 K, stirring under reflux for 24 hours. White crystals were washed with hot DMF at 373 K and acetone, followed by overnight vacuum drying at 423 K.

Characterization

Activated MOF samples (pristine, acid gas exposed and recovered) were characterized to determine the physical and chemical properties. An X'Pert Pro PANalytical diffractometer (CuKα source, λ=0.1541 nm) was used to perform powder X-Ray Diffraction (PXRD) measurements. Cu anode was operated at 45 kV and 40 mA for collecting PXRD patterns with a scan time of 12 step/sec and a step size of 0.0167° 2θ over the range of 5-50° 2θ. Tristar, Micromeritics was used to obtain N_2 adsorption isotherms at 77 K. Brunauer-Emmett-Teller (BET) surface area and t-plot pore volume were evaluated from N_2 adsorption isotherms at 77 K obtained with Micromeritics

Tristar analyzer. *Ex situ* FTIR spectra were collected with a resolution of 4 cm^{-1} using a Thermo Scientific Nicolet iS10 FT-IR equipped with a Smart iTX accessory. EDX measurements were carried out with Hitachi SU 8230 scanning electron microscope.

Synchrotron XRD and PDF Analysis

X-ray pair distribution function (PDF) measurements were performed at beamline 11-ID-B of the Advanced Photon Source. An X-ray wavelength of 0.2113 Å (58.677 keV) was used for all measurements. Measurements were made using a Perkin-Elmer large area detector, with a sample to detector distance of 180 mm. Detector calibration was done using a CeO_2 standard. Prior to measurement, all samples were activated in a vacuum oven at 90 °C for 3 hours. Samples were then packed into 1 mm OD Kapton capillaries and sealed at both ends with epoxy. Pattern integration and calibration were performed using FIT2D software[25]. 1-D patterns were then background subtracted and processed into the reduced pair distribution function, G(r), using PDFGetX3 software[26]. The sine Fourier transform was performed over a k range of 0.8-24 $Å^{-1}$, using a r_{poly} value of 1.2. The PDF plots were normalized with the peak at 2 Å corresponding to the first Zn^{2+} coordination bond.

Acid gas exposure

Activated MOF samples were exposed in a system designed and built to enable acid gas exposure of MOFs. The system consists of two individual lines for acid gas and humidity generation. Acid gas was sourced from cylinders with an acid gas concentration of 1000 ppm SO_2 or NO_2 in N_2. Humidity is generated with a Humidity bottle from Fuel Cell Technologies Inc. Ultra-high purity air was used in the humidity stream. These streams are combined and fed into an exposure unit.

The extent of room temperature exposure for each MOF-acid gas pair is chosen to cause significant degradation observed with loss in pore volume, surface area and crystallinity. Six different exposure protocols were used (**Table S1**, Supporting Information). Exposed samples were reactivated at 453 K and vacuum overnight to desorb any physisorbed entities that will affect later linker replacement and characterization.

Solvent Assisted Crystal Redemption (SACRed)

Around 100 mg of degraded MOF samples were treated with 0.25 M solutions containing the fresh native linker dissolved in an appropriate solvent (**Table S2**). The degraded MOF samples were dispersed in the recovery solutions inside Teflon-lined Parr autoclaves and were incubated in an oven without rotation for 48 hours at 363 K. The recovered crystals were separated from the mother liquor and washed thrice with fresh methanol and air dried at 333 K. Dried samples were vacuum activated at 453 K overnight. In the case of ZIF-90, UiO-66 and UiO-67, the crystals were washed thrice with hot DMF and then washed once with methanol, to remove excess linkers.

Results and Discussion

The crystallinity of pristine, acid gas exposed and recovered MOF samples was characterized by PXRD (**Figure 1**). The extent of exposure is represented in ppm-days (concentration×time). The PXRD data in this figure are normalized with respect to the most intense Bragg peak on a log scale without any offset. The evident upward shift of the baseline in ZIF-8 after exposure to 125 ppm-days of dry NO_2 (**Figure 1a**) implies reduced intensities of crystalline peaks as compared to the background. A broad peak from 7° to 20° in dry NO_2-degraded ZIF-8 indicates diffuse scattering from structurally disordered regions. Similarly, a significant loss in crystallinity is observed ZIF-8 exposed to humid NO_2, ZIF-90 exposed to humid SO_2, and ZIF-71 exposed to dry NO_2 (**Figures**

1b-1d). The two carboxylate linker MOFs (UiO-66 and UiO-67) also show an analogous loss in crystallinity (**Figures 1e-1f**). The broadening of characteristic peaks and loss of higher angle peaks is evident in degraded UiO-67 (**Figure 1f**) indicating the loss of long-range order. At the same time, the retention of characteristic peaks in the exposed samples signifies the presence of partial order of the parent crystals, which enables the effective reconstruction of MOF into the parent topology. These findings are analogous to the relative increase in amorphous background signal observed in ZIF-8 exposed to humid SO_2, indicating structural degradation and disorder[2]. The introduction of defects can help interpret the peak broadening observed in PXRD patterns[27]. A model featuring normally distributed layer position fluctuations in ZIF-8 depicts broadened peaks without significant changes in the PXRD pattern, unlike a model with stacking disorder. This suggests that the peak broadening can be attributed to position disorder introduced with the introduction of dangling acid gas-linker complex with the mean position of atoms unchanged. A downward shift of the baseline of SACRed recovered ZIF-8 is observed (**Figure 1a**). The restoration of long-range order in this material is indicated by the elimination of broad amorphous peak from 7° to 20°. Analogous restoration of long-range order with the downward shift of baseline and renewal/reappearance of higher-angle peak intensities is also observed in the other acid gas-MOF combinations upon application of SACRed (**Figure 1b-1f**). The reappearance of higher angle peaks corresponds to the restoration of long-range order (**Figure 1f**).

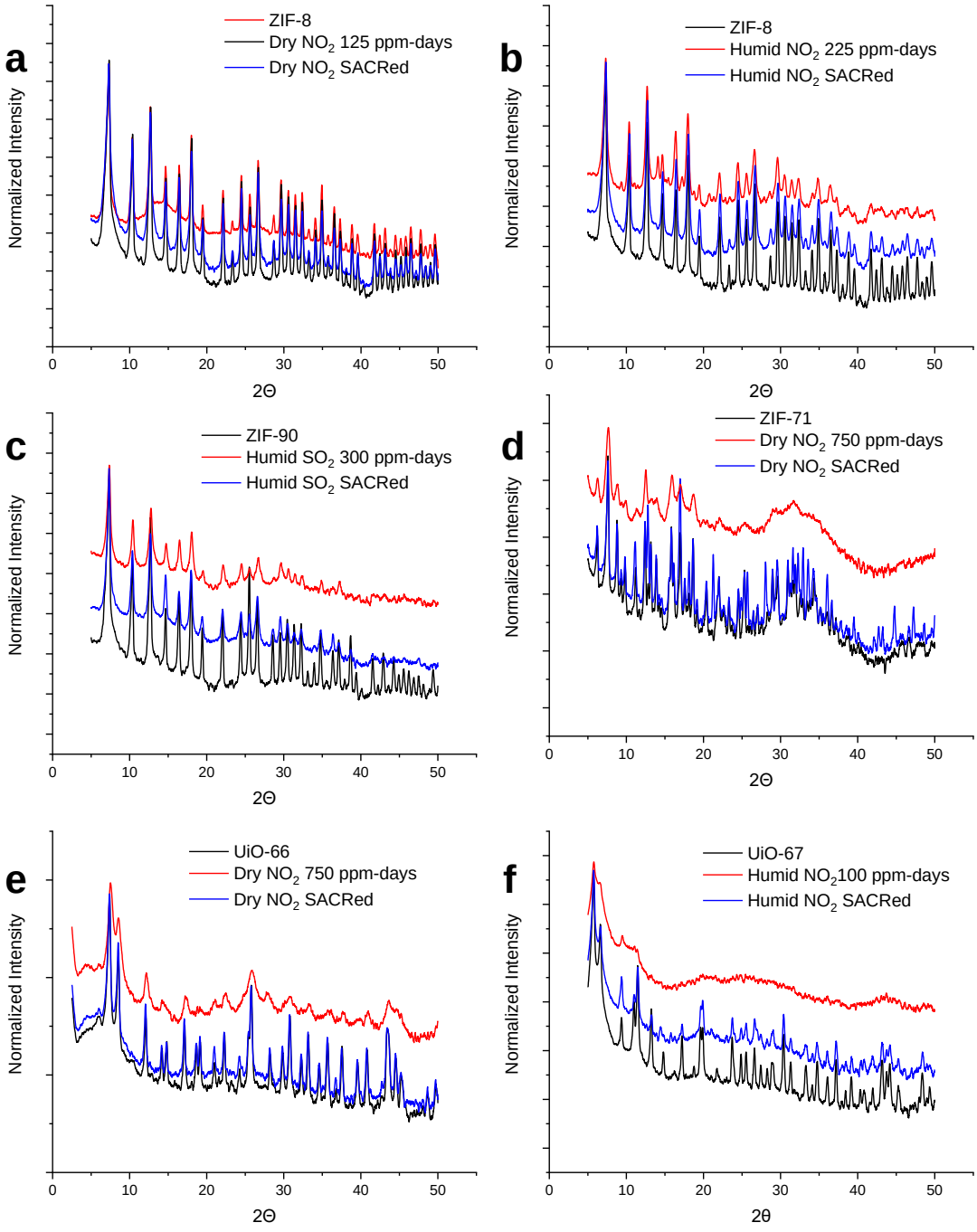

Figure 1. XRD patterns of **(a)** ZIF-8 (pristine, dry NO_2 exposed 125 ppm-days and post SACRed treatment), **(b)** ZIF-8 (pristine, humid NO_2 exposed 225 ppm-days and post SACRed treatment), **(c)** ZIF-90 (pristine, humid SO_2 exposed 300 ppm-days and post SACRed treatment), **(d)** ZIF-71 (pristine, dry NO_2 exposed 750 ppm-days and post SACRed treatment), **(e)** UiO-66 (pristine, dry NO_2 exposed 750 ppm-days and post SACRed treatment) and **(f)** UiO-67 (pristine, humid NO_2 exposed to 100 ppm-days and post SACRed treatment).

Table S3 (Supporting Information) shows the BET surface area and *t*-plot micropore volume for pristine, degraded, and SACRed-recovered MOF materials as obtained from N_2 adsorption isotherms measured at 77 K. In the case of ZIF-8 exposed to dry NO_2, the surface area and pore volume drop to 53% and 59% respectively relative to the pristine ZIF-8. After SACRed treatment, the pore volume (surface area) recovers to 87% (92%) of the original value. Similarly, in humid NO_2 degradation and recovery, pore volume and surface area lowered to 37% and were subsequently restored to 80% of pristine ZIF-8, respectively, indicating that NO_2-damaged linkers can be replaced to a significant extent, similar to the case of ZIF-8 after humid SO_2 degradation[13]. ZIF-90 exposed to humid SO_2 showed an analogous behavior with the exposed sample retaining only 30% of pore characteristics later increasing to 70% of the original surface area and 76% of the original pore volume upon recovery. ZIF-71 and UiO-66 upon dry NO_2 exposure and SACRed recovery display a similar trend. Remarkably, humid NO_2 exposure of UiO-67 leads to the near-complete loss of porosity but SACRed completely restores of the porosity characteristics. Overall, the PXRD patterns and N_2 physisorption data depict different levels of degradation and recovery for each MOF-acid gas pair. This reflects the quite different interactions of different acid gas (e.g., SO_2 versus NO_2) with these MOFs, and the further effects of humidity. Complete recovery of porosity in every case is not pursued in this work for several reasons. Firstly, our objective here is to demonstrate a generalized approach to linker replacement, even if the resulting materials are not completely recovered. Second, NO_2 may have other effects such as functionalizing some of the organic linkers, and SO_2 can react with the aldehyde group in ZIF-90 linkers (2-carboxyimidazole)[28]. While these side-reactions do not degrade the MOFs, they are expected to reduce the pore volume depending on the MOF and the acid gas, due to the addition of the new SO_2 or NO_2 derived functional groups. For example, complete functionalization of the 4-carbon

(or 5-carbon) position in ZIF-8 by -NO_2 groups would reduce its pore volume by ~50% even without any degradation. There is a large SACRed parameter space of linker solution concentrations, temperature, and duration that could be used in SACRed and our aim in this paper is not to exhaustively explore this parameter space.

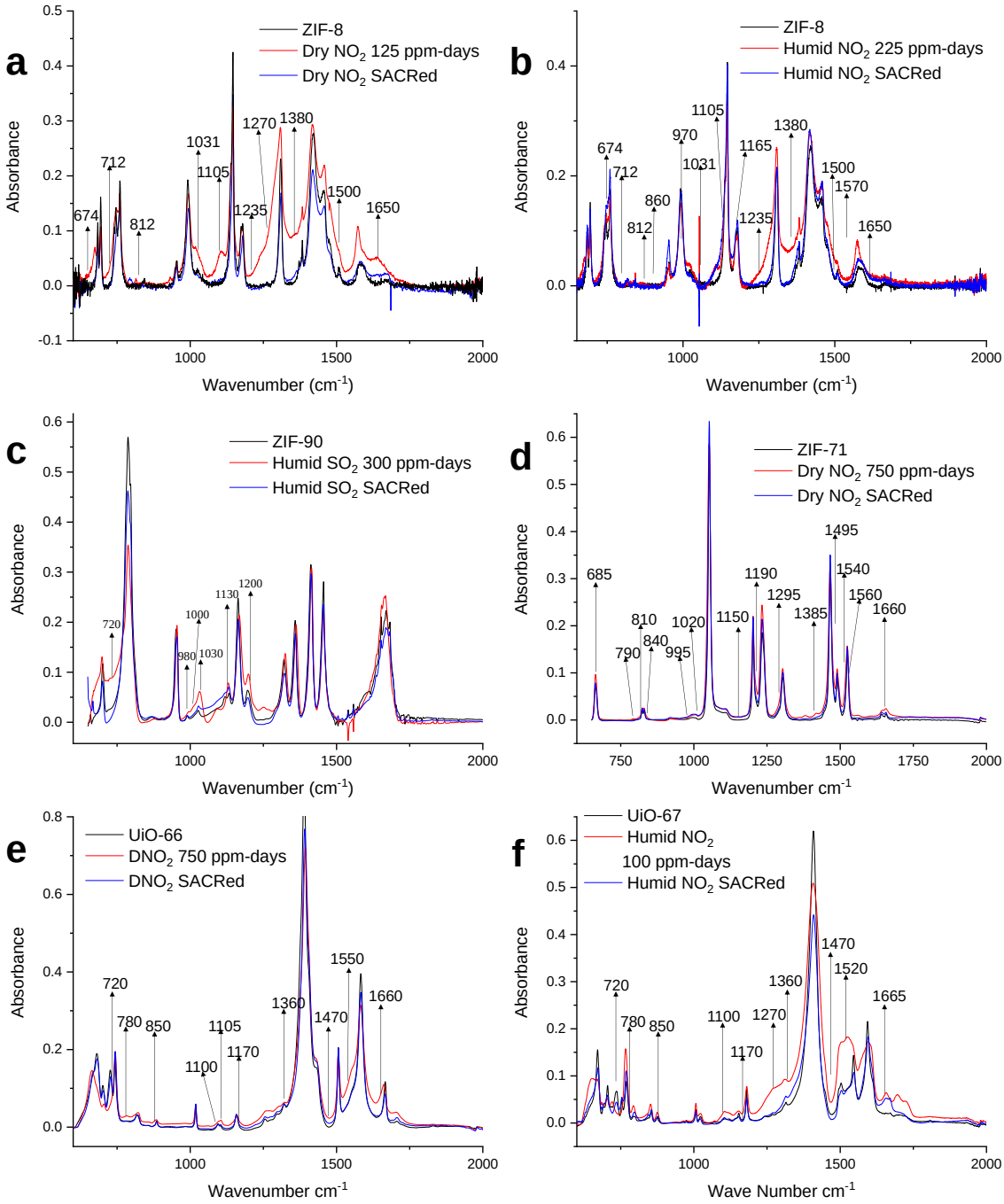

Figure 2. FTIR spectra 600-2000 cm^{-1} of **(a)** ZIF-8 (pristine, dry NO_2 exposed 125 ppm-days and post SACRed treatment), **(b)** ZIF-8 (pristine, humid NO_2 exposed 225 ppm-days and post SACRed treatment), **(c)** ZIF-90 (pristine, humid SO_2 exposed 300 ppm-days and post SACRed treatment), **(d)** ZIF-71 (pristine, dry NO_2 exposed 750 ppm-days and post SACRed treatment), **(e)** UiO-66 (pristine, dry NO_2 exposed 750 ppm-days and post SACRed treatment) and **(f)** UiO-67 (pristine, humid NO_2 exposed to 100 ppm-days and post SACRed treatment).

We used FTIR spectroscopy to track the chemical transformations occurring with acid gas exposure and subsequent SACRed treatment of the six MOFs. This is aided by detailed peak assignments made recently for ZIF-8 exposed to SO_2[1,2] and NO_2[3]. We first summarize the present findings for ZIF-8, which are consistent with previous reports. Overall, a diverse set of organic and inorganic nitrogenic groups are observed in ZIF-8 exposed to dry or humid NO_2 (**Figures 2a-2b**). A peak corresponding to N=O stretch at 1650 cm^{-1} along with additional peaks at 812, 674 and 1105 cm^{-1} (N-O stretch, O-N=O deformation and C-O stretch respectively) confirms the presence of organic nitrites (**Schematic 1d**). Peaks at 1570 cm^{-1} (asymmetric NO_2 stretch), 970 cm^{-1} (N-N stretch), 1500 cm^{-1} (N=O stretch) and 1165 cm^{-1} (C-N stretch) depict the presence of organic nitrosamines and nitramine (**Schematic 1a-1b**) in humid NO_2 exposed ZIF-8, whereas these peaks are absent in the ZIF-8 exposed to dry NO_2[29,30]. The asymmetric NO_2 stretch in the range of 1500-1540 cm^{-1} and the peak at 1031 cm^{-1} (aromatic C-N stretch) indicate the presence of organic nitro- groups (**Schematic 1e**) in humid NO_2-exposed ZIF-8[29,30]. The overlapping nature of these peaks prevents the unambiguous assignment of organic nitro- groups ZIF-8 exposed to dry NO_2. The peak at 1270 cm^{-1} (symmetric NO_2 stretch) indicates a probable presence of organic nitrate (**Schematic 1c**) group in dry NO_2 exposure whereas peaks corresponding to organic nitrate groups are absent when ZIF-8 is exposed to humid NO_2[30]. In ZIF-8 exposed to both dry or humid NO_2, a peak at 812 cm^{-1} along with an additional peak at 1235 cm^{-1} corresponding to asymmetric NO_2 stretch confirms the presence of inorganic nitrite (**Schematic 1f**)[30]. A masked shoulder at 1380 cm^{-1} (symmetric NO_3 stretch) with other characteristic peaks at 712 and 860 cm^{-1} indicate the presence of inorganic nitrates (**Schematic 1g**) after humid NO_2 exposure of ZIF-8[31]. The prence of inorganic nitrite after dry exposure of ZIF-8 cannot be distinctly confirmed due to the overlapping nature of the characteristic peaks. The distinctions in the species formed upon dry

and humid exposure illustrate the mechanistic differences resulting from the absence or presence of water vapor. The functionalization of organic linkers upon exposure is confirmed by the emergence of organic functional groups, while the cleavage of metal-linker bonds is confirmed by the presence of inorganic nitrogenic groups. The cleavage of metal-linker bonds is essential for selective linker replacement (by SACRed), which leads to a substantial reduction or disappearance of peaks corresponding to both organic and inorganic nitrogenic functional groups. However, the post-SACRed peaks at 795, 1355 and 1650 cm^{-1} in dry NO_2-exposed ZIF-8 and peaks at 1100, 1200 and 1640 cm^{-1} in humid NO_2-exposed ZIF-8 confirms the occurrence of organic functionalization of linkers independent of metal-linker bond cleavage.

The FTIR spectra of ZIF-90 exposed to humid SO_2 and subsequently recovered with SACRed treatment are presented in **Figure 2c**, along with that of pristine ZIF-90. The appearance of peaks at 980, 1030 and 1200 in the exposed material correspond to the presence of (bi)sulfites[32]. The appearance of peaks at 720 and 1000 cm^{-1} can be assigned to the formation of sulfites[33,34]. Additionally, overlapping peaks at 960 and 1130 cm^{-1} can be attributed to (bi)sulfites and (bi)sulfates respectively[2]. On the other hand, the FTIR spectrum of SACRed-treated ZIF-90 is a close match with pristine ZIF-90. After the SACRed treatment, a broad peak is present between 1000-1200 cm^{-1} indicating a substantial but not complete recovery, unlike ZIF-8 exposed to humid SO_2[13].

Figure 2d shows the behavior of ZIF-71 upon exposure to dry NO_2 and later recovered with SACRed. ZIF-71 is particularly interesting among ZIFs, since it shows higher resistance than other materials to several types of acid gases[1]. In ZIF-71 exposed to dry NO_2, the presence of organic nitrites (**Schematic 1d**) is shown by the peak at 1660 cm^{-1} assigned to N=O stretch along with the allied peaks at 685, 810 and 1150 cm^{-1} attributed to O-N=O deformation, N-O stretch and C-O

stretch respectively. Peaks corresponding to asymmetric NO_2 stretch and aromatic C-N stretch at 1540 and 1020 cm^{-1} along with a partially overlapping peak at 840 cm^{-1} (NO_2 deformation) indicate a probable presence of organic nitro groups (**Schematic 1e**)[29,30]. The asymmetric NO_2 stretch at 1560 cm^{-1} along with less distinct peaks at 790, 995 and 1295 cm^{-1} assigned to NO_2 deformation, N-N stretch and symmetric NO_2 stretch unambiguously indicate the formation of nitramine (**Schematic 1b**) upon exposure. A shoulder at 1495 cm^{-1} (N=O stretch) and 1190 cm^{-1} (C-N stretch) suggest the presence of nitrosamine (**Schematic 1a**)[29,30]. The formation of inorganic nitrate (**Schematic 1g**) is indicated by peaks at 840 and 1385 cm^{-1} (asymmetric NO_3 stretch)[30]. No signs of inorganic nitrite or organic nitrate are observed. The vibrational changes observed in ZIF-71 are modest compared to ZIF-8, even though the exposure level is six times higher than was used for ZIF-8. Overall, these changes are consistent with the mechanism proposed earlier[3], *i.e.*, degradation during dry NO_2 exposure proceeds via proton abstraction by NO_2. The ZIF-71 linker (4,5-dichloroimidazole has only a single proton available for proton abstraction as compared to five (2 aromatic and 3 aliphatic) in the ZIF-8 linker. Thus, the availability of protons acts as a limiting factor for degradation of ZIF-71 in dry NO_2. The FTIR spectrum of the SACRed-treated ZIF-71 is nearly identical to the pristine material. Small peaks at 1000, 1218 and 1430 cm^{-1} in the recovered samples indicate residual levels of NO_2 derived organic functionalization, consistent with the near-complete recovery as observed in PXRD and N_2 adsorption isotherms.

Turning to the two carboxylate MOFs, UiO-66 and UiO-67, the FTIR spectra after exposure to dry and humid NO_2 indicate the formation of NO_2 functional groups, similar to the observations in ZIF-8 and ZIF-71 (**Figures 2e-2f**). The N=O stretch at 1660 cm^{-1} in both MOFs can be assigned to the formation of organic nitrite groups (**Schematic 2b**). This assignment is supported with N-O stretch and O-N=O deformation peaks around 780 and 1105 cm^{-1} in both MOFs[3]. The asymmetric

NO_2 stretch at 1520 cm^{-1} and aromatic C-N stretch at 1100 cm^{-1} confirm the presence of organic nitro groups (**Schematic 2c**) in UiO-67[29,30]. In the case of UiO-66, peaks at 1550 cm^{-1} (asymmetric NO_2 stretch) and 1100 cm^{-1} (aromatic C-N stretch) with the absence of other allied peaks corresponding to aliphatic C-N stretch and NO_2 deformation indicate a probable presence of organic nitro groups (**Schematic 2c**). A peak at 1655 cm^{-1} assigned to asymmetric NO_2 stretch with other supporting peaks at 1270 cm^{-1} (symmetric NO_2) stretch and NO_2 deformation peaks suggest a probable presence of organic nitrate groups (**Schematic 2a**) in UiO-67[30], whereas such peaks are absent in UiO-66 exposed to dry NO_2. No peaks can unambiguously confirm the formation of nitrosamine and nitramine in both UiO-66 and UiO-67. Shoulder peaks at 1360 cm^{-1} assigned to asymmetric NO_3 stretch with allied peaks at 720 and 850 cm^{-1} confirm the formation of inorganic nitrate groups (**Schematic 2e**) in both UiO-66 and UiO-67[35]. These detailed observations are consistent with more general observations reported earlier[6]. The disappearance of peaks in the range of 600-800 cm^{-1} corresponding to the out-of-plane (oop) bending of aromatic H in the exposed MOFs, supports the same H-abstraction mechanism by NO_2 as prevalent in ZIFs. After SACRed treatment, the peaks corresponding to the organic and inorganic nitro functional groups are significantly decreased in intensity. The out-of-plane bending peaks in the range of 600-800 cm^{-1} are partially restored with recovery. These observations are aligned with the PXRD and N_2 adsorption isotherm results for both UiO-66 and UiO-67.

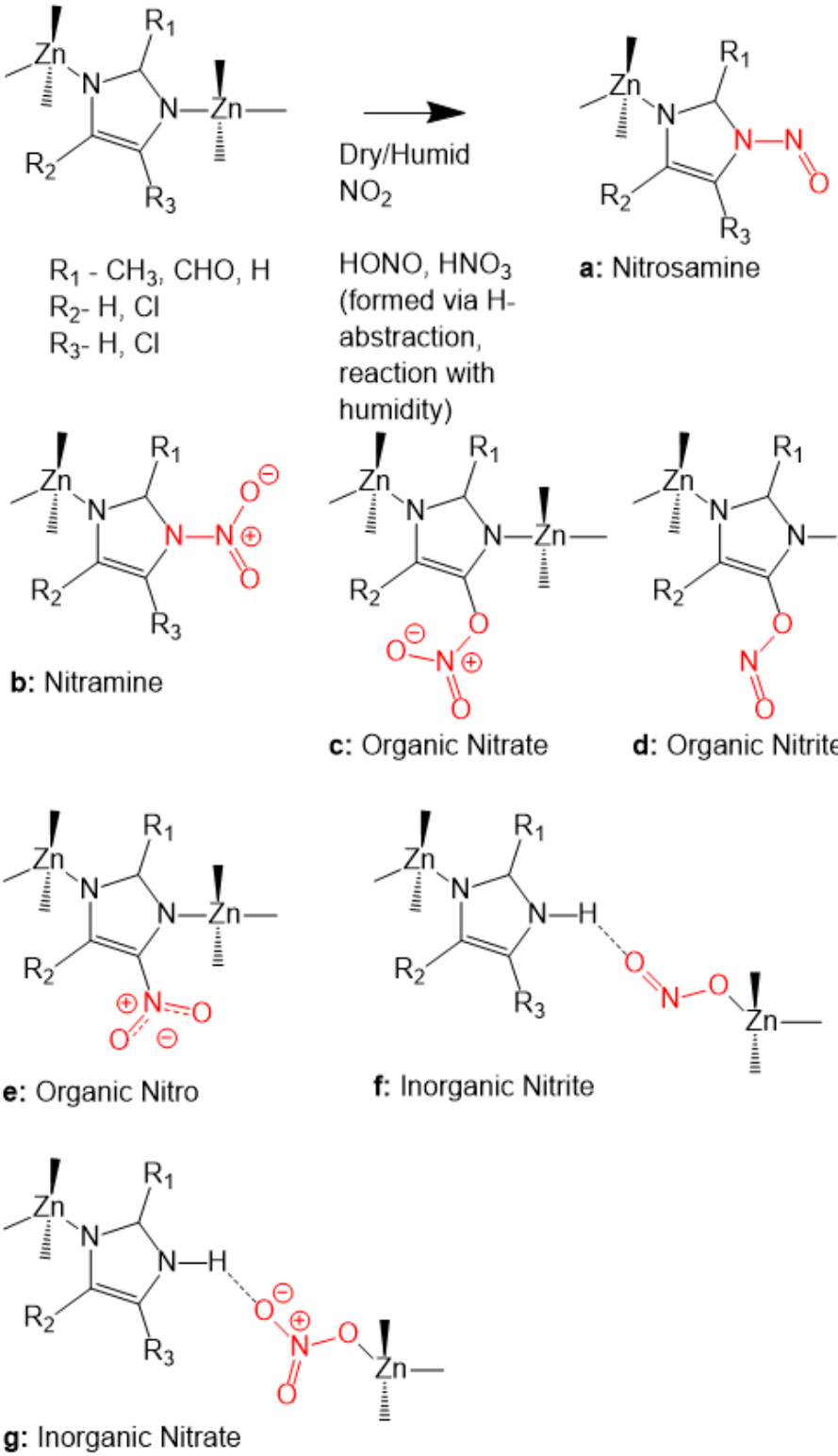

Schematic 1. Product species generated during degradation of ZIFs under dry/humid NO_2. Reaction can occur at any site R_1, R_2, and R_3 (except $R_1 = CH_3$, $R_2/R_3 = Cl$). More detailed examples of stoichiometric reactions have been described in earlier work[3].

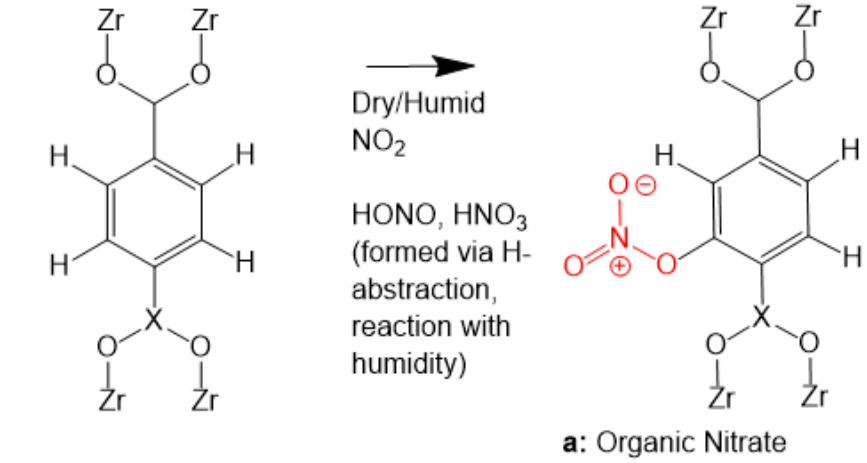

a: Organic Nitrate

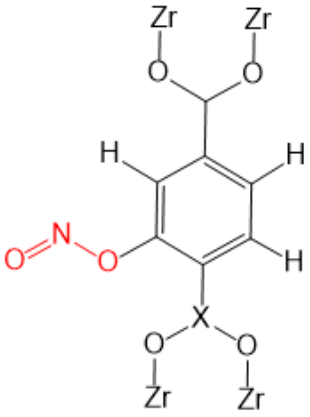

b: Organic Nitrite

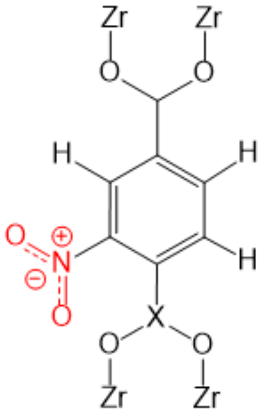

c: Organic Nitro

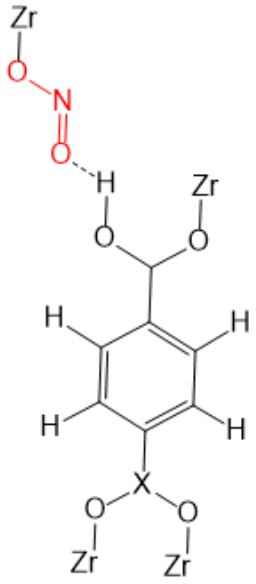

d: Inorganic Nitrite

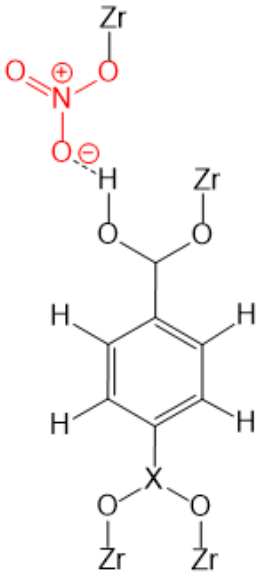

e: Inorganic Nitrate

Schematic 2. Product species generated during degradation of UiOs under dry/humid NO_2. Reaction can occur at any site H-site (X represents carboxylate group in UiO-66 and phenyl carboxylate group in UiO-67).

To provide more detailed insights into the SACRed treatment method, we selected one material (ZIF-8) for further analysis with real space Pair Distribution Functions (PDFs) obtained from high-resolution synchrotron X-ray diffraction data (**Figures 3-4**). **Figure 3** shows the PDFs of ZIF-8 (pristine, dry NO_2 exposed, and SACRed treated). The reduction in the intensity of peaks (which correspond to atomic pair distances) upon exposure indicates the loss of long-range order. For example, the loss of peak intensities in the range of 1-6.4 Å (first Zn coordination sphere) implies the scission of Zn-N (imidazole) bonds leading to inter-molecular level modifications (**Figure 3a**). Similarly, the reduced intensity of peaks at longer distances indicates that the degradation of crystalline order has extended to intra- (6.4-14 Å) and inter-unit cell (14-30 Å) distances (**Figures 3b** and **3c** respectively). Upon SACRed treatment, the ZIF-8 PDFs are restored to become practically identical to the pristine material at all distance ranges (**Figure 3**) shows the restoration of peaks in intermolecular, intra- and inter-unit cell), thus confirming the atomic/molecular level repair and associated renewal of long-range order.

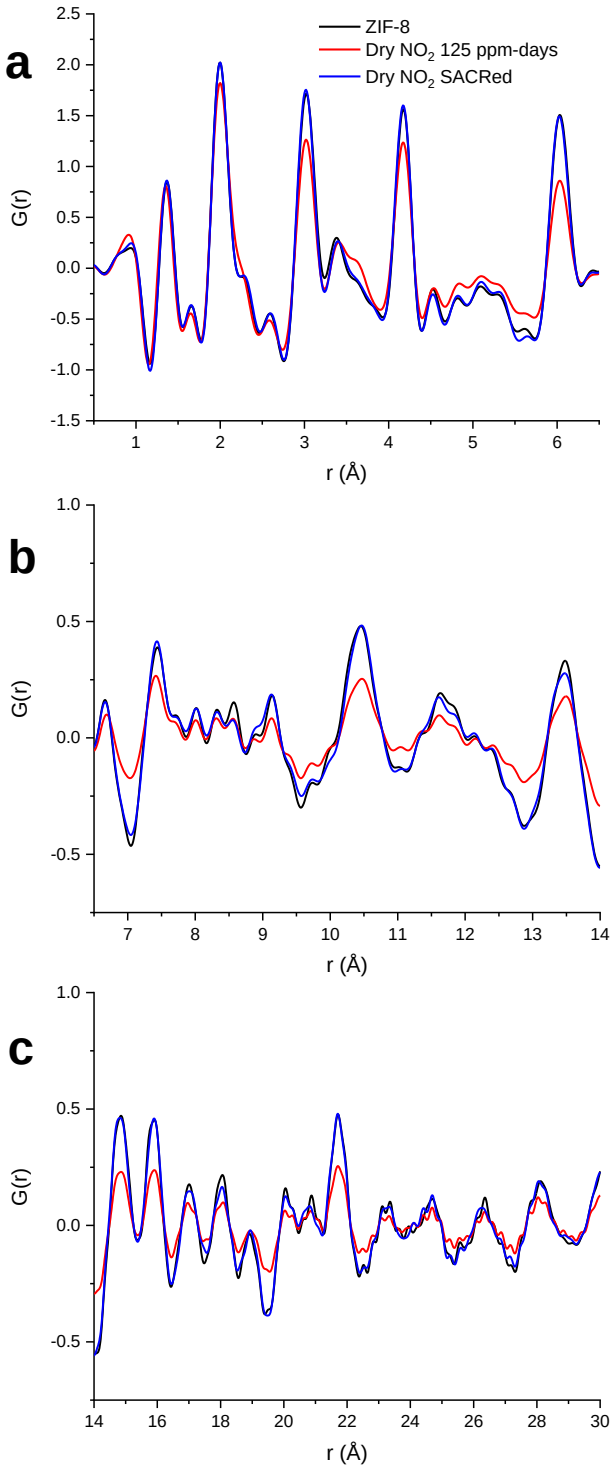

Figure 3. X-Ray Pair Distribution Function (X-Ray PDF) of ZIF-8 (pristine, Dry NO_2 exposed 125 ppm-days and post SACRed treatment) (a) 0-14 Å and (b) 14-30 Å.

Figure 4 shows PDFs for ZIF-8 exposed to 95% humid SO_2 at different total exposure levels (pristine, 100 ppm-days, 140 ppm-days, and 180 ppm-days). The intensity of each atomic-pair peak ($r > 2$ Å) is reduced with increased exposure, illustrating the loss of inter-molecular and long-range order. Peak fitting analysis of the peak corresponding to Zn-N bond (2.01 Å) in pristine ZIF-8 and the emergent Zn-O bond (1.93 Å) in degraded ZIF-8 (created by the incorporation of inorganic sulfite and sulfate) was performed, and provides further insight into the degradation mechanism (**Table 1**). The area of each characteristic peak is a semi-quantitative measure of the number of bonds present. The gradual introduction of Zn-O bonds is depicted with an increased Zn-O/Zn-N ratio upon increased exposure. **Table 2** shows the analysis of the first peak in the PDF pattern (~1.4 Å) which corresponds to C-C and C-N bond lengths. In humid SO_2 exposed ZIF-8, the S=O peaks (from bisulfite and bisulfate species) at 1.5 Å will overlap with this peak. The increased peak area, full width half maximum (FWHM), and the shift of the peak maximum to higher distances, conclusively establish the increased presence of S=O with greater exposure.

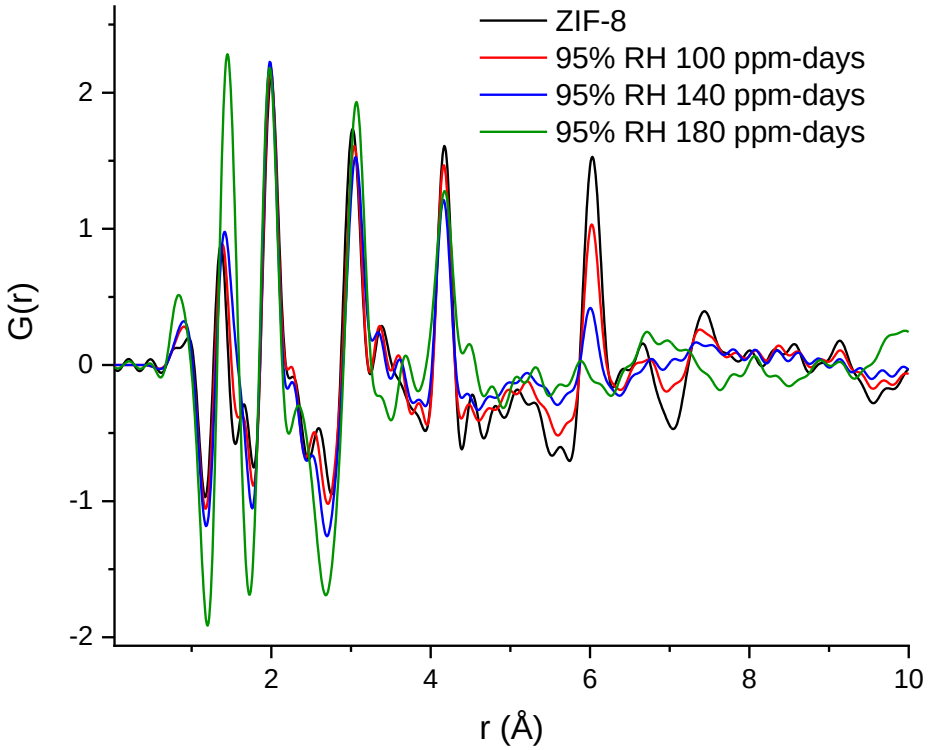

Figure 4. X-Ray Pair Distribution Function (X-Ray PDF) of 95% humid SO_2 exposed ZIF-8 (pristine, 100, 140 and 180 ppm-days)

Table 1. Peak-fitting analysis of Zn-N and Zn-O bonds in pristine and humid SO_2-exposed ZIF-8.

Material	Zn-O		Zn-N		Analysis	
	Peak Position (Å)	**Peak Area (arb. units)**	**Peak Position (Å)**	**Peak Area (arb. units)**	**Area Ratio (Zn-O/Zn-N)**	**Total Area (arb. units)**
Pristine ZIF-8	-	0	2.01	0.777	0	0.777
H-SO_2 100 ppm-days	1.94	0.181	2.02	0.579	0.31	0.76
H-SO_2 140 ppm-days	1.93	0.205	2.01	0.557	0.37	0.762
H-SO_2 180 ppm-days	1.93	0.234	2.01	0.529	0.44	0.763

Table 2. Peak-fitting analysis of C-C and C-N bonds in pristine and humid SO_2-exposed ZIF-8.

Material	Peak Range (Å)	Peak Area (arb. units)	FWHM (Å)	Peak Maximum Position (Å)	Maximum Value (arb. units
Pristine ZIF-8	1.27-1.46	0.105	0.126	1.39	0.805
H-SO_2 100 ppm-days	1.29-1.5	0.115	0.136	1.39	0.879
H-SO_2 140 ppm-days	1.31-1.57	0.157	0.165	1.41	0.973
H-SO_2 180 ppm-days	1.32-1.59	0.39	0.178	1.45	2.28

Using ZIFs as an example, we have previously established that SACRed is truly a crystal repair process and does not involve significant dissolution and recrystallization processes[13]. SACRed operates at conditions that are much milder than those required for dissolution, and the preservation of the micrometer-scale morphology of ZIF-8 crystals in the absence of any coordination modulators (such as sodium formate) also confirms that SACRed is a true repair mechanism. Here, we have extended this analysis to carboxylate MOFs using UiO-67. **Figure S2** shows energy-dispersive x-ray (EDX) elemental composition measurements of the UiO-67 synthesis solution used in this work (**Figure S2a**) and the UiO-67 SACRed recovery solution (after 24 hours of treatment, **Figure S2b**), dried over conductive carbon tape. Zr (24.3 atomic% on dry mass basis) is easily detected in the UiO-67 synthesis solution, whereas the UiO-67 SACRed solution does not show any Zr above noise levels. Similar to the case of ZIF-8, this finding strongly supports a true crystal repair mechanism.

Conclusion

Previous demonstrations of SACRed have focused on ZIFs that were degraded by exposure to gas streams containing humid SO_2. In this paper we have extended the use of SACRed to imidazole-based MOFs and carboxylic-based MOFs (UiO-66 and UiO-67) degraded by two different acid

gases (SO_2 and NO_2) under both dry and humid conditions. Our results suggest that SACRed is a versatile technique for introducing new linkers into MOFs after deliberate degradation by acid gases, resulting in highly crystalline materials. In each example we studied the linkers that were introduced had the same identity as the original MOF, but we note that previous studies have shown that SACRed can readily be used to produce mixed linker MOFs[17].

The loss of crystallinity that occurs during exposure to acid gases can be attributed to structural disintegration due to the formation of dangling acid gas- linker complexes[2,4]. The different extent of exposure required to cause observable degradation in each MOF – acid gas pair hints at the complexity of MOF- acid gas interactions and the nontrivial role of humidity in these processes. FTIR analysis of both degraded and recovered samples indicate the formation of dangling linkers during degradation and their subsequent removal during the recovery. FTIR also confirms a diverse set of acid gas-derived organic functionalization of linkers in exposed MOFs. In some cases these functional groups can be formed via acid-gas interactions with intact linkers. These intact functionalized linkers can lead to low levels of porosity loss that cannot be recovered via SACred. In addition to our observations with FTIR, molecular level degradation associated with the formation of dangling acid gas- linker complex upon exposure and the subsequent removal of such complexes have been semi-quantitatively confirmed with X-ray Pair Distribution Function analysis.

References

(1) Bhattacharyya, S.; Han, R.; Kim, W. G.; Chiang, Y.; Jayachandrababu, K. C.; Hungerford, J. T.; Dutzer, M. R.; Ma, C.; Walton, K. S.; Sholl, D. S.; Nair, S. Acid Gas Stability of Zeolitic Imidazolate Frameworks: Generalized Kinetic and Thermodynamic Characteristics. *Chemistry of Materials* **2018**, *30* (12), 4089–4101. https://doi.org/10.1021/acs.chemmater.8b01394.

(2) Bhattacharyya, S.; Pang, S. H.; Dutzer, M. R.; Lively, R. P.; Walton, K. S.; Sholl, D. S.; Nair, S. Interactions of SO_2-Containing Acid Gases with ZIF-8: Structural Changes and Mechanistic Investigations. *Journal of Physical Chemistry C* **2016**, *120* (48), 27221–27229. https://doi.org/10.1021/acs.jpcc.6b09197.

(3) Bhattacharyya, S.; Han, R.; Joshi, J. N.; Zhu, G.; Lively, R. P.; Walton, K. S.; Sholl, D. S.; Nair, S. Stability of Zeolitic Imidazolate Frameworks in NO_2. *Journal of Physical Chemistry C* **2019**, *123* (4), 2336–2346. https://doi.org/10.1021/acs.jpcc.8b11377.

(4) Mounfield, W. P.; Han, C.; Pang, S. H.; Tumuluri, U.; Jiao, Y.; Bhattacharyya, S.; Dutzer, M. R.; Nair, S.; Wu, Z.; Lively, R. P.; Sholl, D. S.; Walton, K. S. Synergistic Effects of Water and SO_2 on Degradation of MIL-125 in the Presence of Acid Gases. *Journal of Physical Chemistry C* **2016**, *120* (48), 27230–27240. https://doi.org/10.1021/acs.jpcc.6b09264.

(5) Bhattacharyya, S.; Sholl, D. S.; Nair, S. Quantitative Correlations for the Durability of Zeolitic Imidazolate Frameworks in Humid SO_2. *Industrial and Engineering Chemistry Research* **2020**, *59* (1), 245–252. https://doi.org/10.1021/acs.iecr.9b05787.

(6) Ebrahim, A. M.; Levasseur, B.; Bandosz, T. J. Interactions of NO_2 with Zr-Based MOF: Effects of the Size of Organic Linkers on NO_2 Adsorption at Ambient Conditions. *Langmuir* **2013**, *29* (1), 168–174. https://doi.org/10.1021/la302869m.

(7) Decoste, J. B.; Peterson, G. W. Metal-Organic Frameworks for Air Purification of Toxic Chemicals. *Chemical Reviews* **2014**, *114* (11), 5695–5727. https://doi.org/10.1021/cr4006473.

(8) Bobbitt, N. S.; Mendonca, M. L.; Howarth, A. J.; Islamoglu, T.; Hupp, J. T.; Farha, O. K.; Snurr, R. Q. Metal-Organic Frameworks for the Removal of Toxic Industrial Chemicals and Chemical Warfare Agents. *Chemical Society Reviews* **2017**, *46* (11), 3357–3385. https://doi.org/10.1039/c7cs00108h.

(9) Petit, C.; Mendoza, B.; Bandosz, T. J. Hydrogen Sulfide Adsorption on MOFs and MOF/Graphite Oxide Composites. *ChemPhysChem* **2010**, *11* (17), 3678–3684. https://doi.org/10.1002/cphc.201000689.

(10) Ebrahim, A. M.; Bandosz, T. J. Effect of Amine Modification on the Properties of Zirconium-Carboxylic Acid Based Materials and Their Applications as NO2 Adsorbents at Ambient Conditions. *Microporous and Mesoporous Materials* **2014**, *188* (2), 149–162. https://doi.org/10.1016/j.micromeso.2014.01.009.

(11) Burtch, N. C.; Jasuja, H.; Walton, K. S. Water Stability and Adsorption in Metal-Organic Frameworks. *Chemical Reviews* **2014**, *114* (20), 10575–10612. https://doi.org/10.1021/cr5002589.

(12) Zhang, C.; Han, C.; Sholl, D. S.; Schmidt, J. R. Computational Characterization of Defects in Metal-Organic Frameworks: Spontaneous and Water-Induced Point Defects in ZIF-8. *Journal of Physical Chemistry Letters* **2016**, *7* (3), 459–464. https://doi.org/10.1021/acs.jpclett.5b02683.

(13) Jayachandrababu, K. C.; Bhattacharyya, S.; Chiang, Y.; Sholl, D. S.; Nair, S. Recovery of Acid-Gas-Degraded Zeolitic Imidazolate Frameworks by Solvent-Assisted Crystal Redemption (SACRed). *ACS Applied Materials and Interfaces* **2017**, *9* (40), 34597–34602. https://doi.org/10.1021/acsami.7b11686.

(14) Zhang, X.; Zhang, K.; Yoo, H.; Lee, Y. Machine Learning-Driven Discovery of Metal-Organic Frameworks for Efficient CO_2 Capture in Humid Condition. *ACS Sustainable Chemistry and Engineering* **2021**, *9* (7), 2872–2879. https://doi.org/10.1021/acssuschemeng.0c08806.

(15) Civalleri, B.; Napoli, F.; Noël, Y.; Roetti, C.; Dovesi, R. Ab-Initio Prediction of Materials Properties with CRYSTAL: MOF-5 as a Case Study. *CrystEngComm* **2006**, *8* (5), 364–371. https://doi.org/10.1039/b603150c.

(16) Pillai, R. S.; Suresh, C. H. Computational Prediction of Promising Pyrazine and Bipyridine Analogues of a Fluorinated MOF Platform, MFN-Ni-L (M = SI/AL; N = SIX/FIVE; L = Pyr/Bipyr), for CO_2 Capture under Pre-Humidified Conditions. *Physical Chemistry Chemical Physics* **2019**, *21* (29), 16127–16136. https://doi.org/10.1039/c9cp00845d.

(17) Jayachandrababu, K. C.; Chiang, Y.; Zhang, F.; Korde, A.; Han, R.; Bhattacharyya, S.; Sholl, D. S.; Nair, S. Synthesizing New Hybrid Zeolitic Imidazolate Frameworks by Controlled Demolition and Reconstruction. *ACS Materials Letters* **2019**, *1* (4), 447–451. https://doi.org/10.1021/acsmaterialslett.9b00211.

(18) Thompson, J. A.; Blad, C. R.; Brunelli, N. A.; Lydon, M. E.; Lively, R. P.; Jones, C. W.; Nair, S. Hybrid Zeolitic Imidazolate Frameworks: Controlling Framework Porosity and Functionality by Mixed-Linker Synthesis. *Chemistry of Materials* **2012**, *24* (10), 1930–1936. https://doi.org/10.1021/cm3006953.

(19) Takaishi, S.; Demarco, E. J.; Pellin, M. J.; Farha, O. K.; Hupp, J. T. Solvent-Assisted Linker Exchange (SALE) and Post-Assembly Metallation in Porphyrinic Metal-Organic Framework Materials. *Chemical Science* **2013**, *4* (4), 1509–1513. https://doi.org/10.1039/c2sc21516k.

(20) Zhang, C.; Lively, R. P.; Zhang, K.; Johnson, J. R.; Karvan, O.; Koros, W. J. Unexpected Molecular Sieving Properties of Zeolitic Imidazolate Framework-8. *Journal of Physical Chemistry Letters* **2012**, *3* (16), 2130–2134. https://doi.org/10.1021/jz300855a.

(21) Gee, J. A.; Chung, J.; Nair, S.; Sholl, D. S. Adsorption and Diffusion of Small Alcohols in Zeolitic Imidazolate Frameworks ZIF-8 and ZIF-90. *Journal of Physical Chemistry C* **2013**, *117* (6), 3169–3176. https://doi.org/10.1021/jp312489w.

(22) Zhang, K.; Lively, R. P.; Dose, M. E.; Brown, A. J.; Zhang, C.; Chung, J.; Nair, S.; Koros, W. J.; Chance, R. R. Alcohol and Water Adsorption in Zeolitic Imidazolate Frameworks. *Chemical Communications* **2013**, *49* (31), 3245–3247. https://doi.org/10.1039/c3cc39116g.

(23) Liu, X.; Demir, N. K.; Wu, Z.; Li, K. Highly Water-Stable Zirconium Metal-Organic Framework UiO-66 Membranes Supported on Alumina Hollow Fibers for Desalination. *Journal of the American Chemical Society* **2015**, *137* (22), 6999–7002. https://doi.org/10.1021/jacs.5b02276.

(24) Kaur, G.; Øien-ØDegaard, S.; Lazzarini, A.; Chavan, S. M.; Bordiga, S.; Lillerud, K. P.; Olsbye, U. Controlling the Synthesis of Metal-Organic Framework UiO-67 by Tuning Its Kinetic Driving Force. *Crystal Growth and Design* **2019**, *19* (8), 4246–4251. https://doi.org/10.1021/acs.cgd.9b00916.

(25) Hammersley, A. P.; Svensson, S. O.; Hanfland, M.; Fitch, A. N.; Hausermann, D. Two-Dimensional Detector Software: From Real Detector to Idealised Image or Two-Theta Scan. *High Pressure Research* **1996**, *14* (4–6), 235–248. https://doi.org/10.1080/08957959608201408.

(26) Juhás, P.; Davis, T.; Farrow, C. L.; Billinge, S. J. L. PDFgetX3: A Rapid and Highly Automatable Program for Processing Powder Diffraction Data into Total Scattering Pair Distribution Functions.

Journal of Applied Crystallography **2013**, *46* (2), 560–566. https://doi.org/10.1107/S0021889813005190.

(27) Metz, P. C.; Purdy, S. C.; Ryder, M. R.; Ganesan, A.; Nair, S.; Page, K. Detailed Total Scattering Analysis of Disorder in ZIF-8. *Journal of Applied Crystallography* **2021**, *54* (3), 1–9. https://doi.org/10.1107/s1600576721002843.

(28) Munger, J. W.; Jacob, D. J.; Hoffmann, M. R. The Occurrence of Bisulfite-Aldehyde Addition Products in Fog- and Cloudwater. *Journal of Atmospheric Chemistry* **1984**, *1* (4), 335–350. https://doi.org/10.1007/BF00053799.

(29) Akhter, M. S.; Chughtai, A. R.; Smith, D. M. Reaction of Hexane Soot with NO2/N2O4. *Journal of Physical Chemistry* **1984**, *88* (22), 5334–5342. https://doi.org/10.1021/j150666a046.

(30) Infrared and Raman Characteristic Group Frequencies: Tables and Charts, 3rd Edition | Wiley https://www.wiley.com/en-us/Infrared+and+Raman+Characteristic+Group+Frequencies%3A+Tables+and+Charts%2C+3rd+Edition-p-9780470093078 (accessed Feb 21, 2021).

(31) Li, P.; Xu, Z. P.; Hampton, M. A.; Vu, D. T.; Huang, L.; Rudolph, V.; Nguyen, A. V. Control Preparation of Zinc Hydroxide Nitrate Nanocrystals and Examination of the Chemical and Structural Stability. *Journal of Physical Chemistry C* **2012**, *116* (18), 10325–10332. https://doi.org/10.1021/jp300045u.

(32) Miller, F. A.; Wilkins, C. H. Infrared Spectra and Characteristic Frequencies of Inorganic Ions. *Analytical Chemistry* **1952**, *24* (8), 1253–1294. https://doi.org/10.1021/ac60068a007.

(33) Siriwardan, R. V.; Woodruff, S. FTIR Characterization of the Interaction of Oxygen with Zinc Sulfide. *Industrial and Engineering Chemistry Research* **1995**, *34* (2), 699–702. https://doi.org/10.1021/ie00041a032.

(34) Siriwardane, R. V.; Woodruff, S. In Situ Fourier Transform Infrared Characterization of Sulfur Species Resulting from the Reaction of Water Vapor and Oxygen with Zinc Sulfide. *Industrial and Engineering Chemistry Research* **1997**, *36* (12), 5277–5281. https://doi.org/10.1021/ie970343e.

(35) Levasseur, B.; Ebrahim, A. M.; Burress, J.; Bandosz, T. J. Interactions of NO_2 at Ambient Temperature with Cerium-Zirconium Mixed Oxides Supported on SBA-15. *Journal of Hazardous Materials* **2011**, *197* (2), 294–303. https://doi.org/10.1016/j.jhazmat.2011.09.087.